BAMS Article

Eye of the Storm

Observing Hurricanes with a Small Unmanned Aircraft System

Joseph J. Cione, George H. Bryan, Ronald Dobosy, Jun A. Zhang, Gijs de Boer, Altug Aksoy, Joshua B. Wadler, Evan A. Kalina, Brittany A. Dahl, Kelly Ryan, Jonathan Neuhaus, Ed Dumas, Frank D. Marks, Aaron M. Farber, Terry Hock, and Xiaomin Chen

ABSTRACT: Unique data from seven flights of the Coyote small unmanned aircraft system (sUAS) were collected in Hurricanes Maria (2017) and Michael (2018). Using NOAA's P-3 reconnaissance aircraft as a deployment vehicle, the sUAS collected high-frequency (>1 Hz) measurements in the turbulent boundary layer of hurricane eyewalls, including measurements of wind speed, wind direction, pressure, temperature, moisture, and sea surface temperature, which are valuable for advancing knowledge of hurricane structure and the process of hurricane intensification. This study presents an overview of the sUAS system and preliminary analyses that were enabled by these unique data. Among the most notable results are measurements of turbulence kinetic energy and momentum flux for the first time at low levels (<150 m) in a hurricane eyewall. At higher altitudes and lower wind speeds, where data were collected from previous flights of the NOAA P-3, the Coyote sUAS momentum flux values are encouragingly similar, thus demonstrating the ability of an sUAS to measure important turbulence properties in hurricane boundary layers. Analyses from a large-eddy simulation (LES) are used to place the Coyote measurements into context of the complicated high-wind eyewall region. Thermodynamic data are also used to evaluate the operational HWRF model, showing a cool, dry, and thermodynamically unstable bias near the surface. Preliminary data assimilation experiments also show how sUAS data can be used to improve analyses of storm structure. These results highlight the potential of sUAS operations in hurricanes and suggest opportunities for future work using these promising new observing platforms.

https://doi.org/10.1175/BAMS-D-19-0169.1
Corresponding author: Joseph J. Cione, joe.cione@noaa.gov
In final form 30 October 2019

AFFILIATIONS: Cione,* Marks, and Chen—NOAA/AOML/Hurricane Research Division, Miami, Florida; **Bryan and Hock**—National Center for Atmospheric Research, Boulder, Colorado; **Dobosy, and Dumas**—NOAA/ARL/Atmospheric Turbulence and Diffusion Division, and Oak Ridge Associated Universities, Oak Ridge, Tennessee; **Zhang, Aksoy, Dahl, and Ryan**—NOAA/AOML/Hurricane Research Division, and Cooperative Institute for Marine and Atmospheric Studies, University of Miami, Miami, Florida; **de Boer**—Cooperative Institute for Research in Environmental Sciences, University of Colorado Boulder, Boulder, Colorado; **Wadler**—Rosenstiel School of Marine and Atmospheric Science, University of Miami, Miami, Florida; **Kalina**—Cooperative Institute for Research in Environmental Sciences, University of Colorado Boulder, and Developmental Testbed Center, and NOAA Global Systems Division, Boulder, Colorado; **Neuhaus**—NOAA/OMAO/Aircraft Operations Center, Lakeland, Florida; **Farber**—L3 Latitude, Tucson, Arizona
*** CURRENT AFFILIATION: Cione**—NOAA/AOML/Hurricane Research Division, Miami, Florida

Hurricanes are well known for the strong wind speeds they produce and the damage they can cause (e.g., Emanuel 2005; Pielke and Landsea 1998, 1999; Pielke et al. 2008; Klotzbach et al. 2018). However, high-resolution measurements of winds and thermodynamic properties in strong hurricanes are rare below 2-km altitude. In situ anemometers can be damaged by hurricane-force winds and only infrequently encounter the inner core of a hurricane where the strongest winds occur. Reconnaissance aircraft, such as the NOAA WP-3D ("P-3"; Aberson et al. 2006a) have rarely flown below ~2 km through a hurricane's strongest winds (e.g., Marks et al. 2008; Zhang et al. 2011b; Zhang and Montgomery 2012), and safety concerns have precluded such low-level flights in hurricanes in the last decade. Doppler radars provide high-value information within hurricanes, including data from the NOAA P-3 Tail Doppler Radar (TDR; Jorgensen et al. 1983), and from mobile ground-based radars within landfalling storms (e.g., Wurman and Kosiba 2018). Also, over the last 20 years, GPS dropsondes (Hock and Franklin 1999) have been used to obtain high-resolution, nearly vertical profiles of wind speed, wind direction, temperature, humidity, and pressure, which have provided key insights into hurricane structure (e.g., Zhang et al. 2011a) and wind gusts (e.g., Stern et al. 2016) and provide no measure of horizontal variability. Despite these advances, additional high-resolution measurements in hurricanes are still needed at altitudes below 1 km to adequately assess the properties of turbulence in hurricanes, including gust factor and turbulence intensity (e.g., Harper et al. 2010), which are crucial for future advances in applications such as numerical modeling systems (e.g., Smith and Thomsen 2010; Zhang et al. 2015) and wind-energy assessments (e.g., Worsnop et al. 2017a).

In recent years, observations from unmanned aircraft systems (UAS) have increasingly contributed to atmospheric understanding as the technology has become increasingly affordable and reliable. Small UAS (sUAS; defined by the Federal Aviation Administration as those that weigh less than 25 kg) are particularly useful in hazardous conditions because they provide benefits of low cost and simple operability. A thorough review of sUAS for general meteorological applications is provided in Elston et al. (2015).

Within hurricanes, the use of sUAS has been limited and only a small number of preliminary missions are reported in the literature. One such aircraft is the Aerosonde (Holland et al. 1992), which was flown into various tropical cyclones (TCs). The observation characteristics from the Aerosonde were reported for Tropical Storm Ophelia (2005) by Cione et al. (2008) and Cascella et al. (2008), for Typhoon Longwang (2005) by Lin and Lee (2008), and for Hurricane Noel (2007) by Cascella et al. (2008). While the Aerosonde hurricane flights provided unique

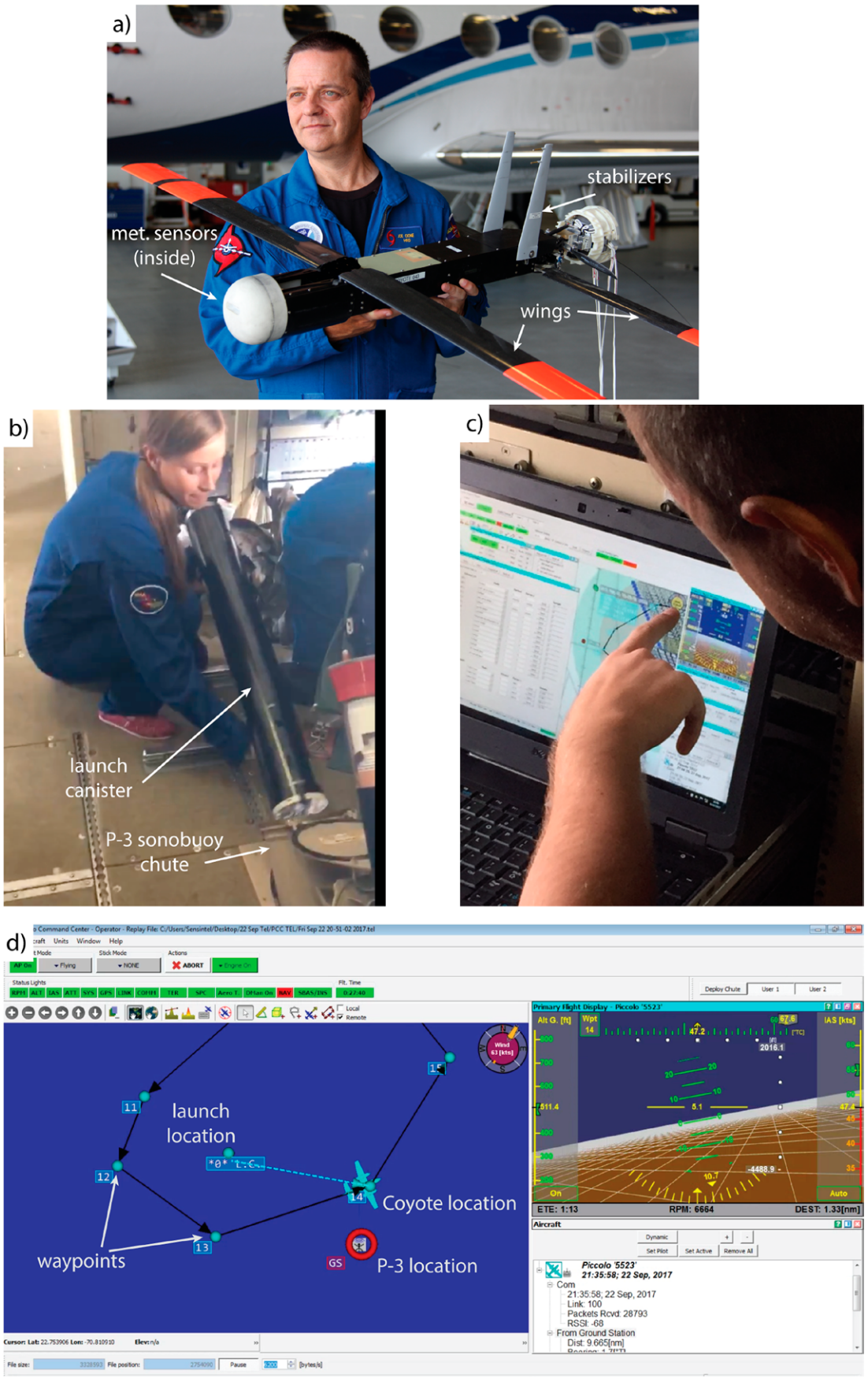

Fig. 1. Pictures of the Coyote aircraft and Coyote sUAS operations. (a) J. Cione holding a Coyote drone at NOAA's Aircraft Operations Center with key features annotated. (b) K. Ryan launching a Coyote drone from a NOAA P-3 aircraft. (c) A photograph of operations during a Coyote flight. (d) A screen capture from the Coyote operator's software; the Coyote drone has an onboard autopilot, but the operator provides "waypoints" to fly toward.

datasets, the vehicle was launched and controlled from land, which resulted in long ferry times and limited its potential use for TC research and operations.

More recently, a new type of sUAS called the Coyote (Fig. 1a) was deployed successfully in Hurricane Edouard (2014) from the NOAA P-3 (Cione et al. 2016). Launching the sUAS from the P-3 within a TC allows for improved sampling in the area of greatest interest, particularly the planetary boundary layer (PBL; roughly the lowest 1 km in hurricanes) and at high wind speeds (roughly greater than 30 m s^{-1}), without the need for long ferry times by the UAS.

Measurements by sUAS at low altitudes can provide insight into processes that influence hurricane intensity and intensity change. For example, these observations can be used to quantify air–sea fluxes of latent and sensible heat, and momentum, which have uncertain values but are known to play a key role in hurricane maximum intensity (e.g., Emanuel 1995; Bryan 2012) and intensification rate (e.g., Montgomery et al. 2010; Bryan 2013). These surface fluxes have been estimated using low-level flight data obtained using NOAA's P-3 (French et al. 2007; Drennan et al. 2007), although only at tropical-storm-force wind speeds. A few flux measurements have been made at hurricane-force wind speeds (e.g., Zhang et al. 2011b), but these have been too far from the surface to use for estimating surface fluxes.

Above the surface, turbulence processes in the entire PBL are also important for hurricane structure and intensification (e.g., Smith and Thomsen 2010), although measurements of variables such as effective eddy diffusivity at high wind speeds is a fundamental gap in the TC literature. In general, a greater understanding of temporal and spatial variability of PBL properties is needed to support and verify previous observational, modeling, and theoretical studies (e.g., Emanuel 1995; Braun and Tao 2000; Nolan et al. 2009a,b; Smith and Thomsen 2010; Bryan 2012; Bell et al. 2012; Kepert 2012; Cione et al. 2013; Zhang et al. 2017; Chen et al. 2018; Wadler et al. 2018). A comprehensive review on boundary layer process, and their effects on hurricane dynamics, was recently published by Montgomery and Smith (2017).

Data collected by the Coyote can also be used to evaluate hurricane forecasting tools, such as NOAA's Hurricane Weather Research and Forecasting (HWRF) system. Although HWRF intensity forecasts have substantially improved in recent years because of improved physics packages (Gall et al. 2013; Tallapragada et al. 2014; Zhang et al. 2018), the current PBL parameterization is based on a limited number of in situ observations (e.g., Zhang et al. 2015). sUAS platforms offer a unique opportunity to collect additional measurements within hurricanes that are needed to improve physical parameterizations, as advocated by Smith and Thomsen (2010).

This paper provides an overview of recent Coyote sUAS deployments in Hurricanes Maria (2017) and Michael (2018). These flights include the first direct measurements of turbulence properties at low levels (below 150 m) in a hurricane eyewall. In addition, preliminary analyses are presented of how sUAS data can be used to evaluate numerical models. These results highlight ongoing work with sUAS data collected in hurricanes, and suggest opportunities for future work using these promising new observing platforms.

Description of Coyote sUAS operations in hurricanes

Deployment of the Coyote. The work in this article was conducted using the Coyote sUAS (Fig. 1a), which is built and supported by the Raytheon Company. Technical details of the Coyote sUAS are provided in the sidebar. The Coyote is an air-launched aircraft, originally developed for military applications, that has recently been adapted for meteorological research. It features a folding wing set that allows the Coyote to fit in a standard A-size sonobuoy launch canister (Fig. 1b). No modifications to the NOAA P-3s were necessary because they already had the capability to release sonobuoys.

The launch and deployment sequence of a Coyote is illustrated in Fig. 2. The device exits the P-3 initially in free fall (Fig. 2a), but quickly deploys a parachute to slow descent and reduce rotation (Fig. 2b). After the position of the cylinder stabilizes (after ~15 s), the external

The Coyote small unmanned aircraft system

The Coyote is a small unmanned aircraft system (sUAS) produced by the Raytheon Company. The wings and stabilizers fold inward toward the fuselage so, when stowed, the Coyote fits in a standard A-size sonobuoy launch canister (Figs. 1b and 2b). When deployed, the Coyote's wingspan is 1.5 m and its length is 0.9 m (Fig. 1a). Its weight is 6 kg and it can carry a payload up to 1.8 kg. In flight, the Coyote uses an electric pusher motor, leaving minimally disturbed air for sampling at the nose. The cruising airspeed is 28 m s^{-1}.

The main wings and vertical stabilizers have no control surfaces; rather, the Coyote uses elevons (i.e., combined elevator and aileron) which are on the rear wings and are controlled by a Cloud Cap Technologies Piccolo Nano autopilot. The GPS-guided Piccolo autopilot system contains internal accelerometers and gyros to help keep the aircraft level and on track.

Data were transmitted from the Coyote in real time and were received on the NOAA P-3 aircraft. For all of these flights, some data were also transmitted in near–real time to NOAA's National Hurricane Center (NHC) and in some instances the data were noted in NHC advisories. A major shortcoming of initial Coyote flights in Hurricane Edouard (2014) was a limited range of ~10 km that the P-3 needed to maintain in order to receive sUAS data (Cione et al. 2016). For operations beginning in 2017, a 350-MHz data link was used, which improved the range of the Coyote substantially and allowed the P-3 to execute normal flight paths. Use of the 350-MHz radio frequency also substantially improved data collection, from ~7% of data received during flights in the eyewall of Hurricane Edouard (Cione et al. 2016) to >90% data collection in the eyewall of Hurricane Maria.

For the Coyote flights described in this study, an International Met Systems (iMet) XF system was used to measure thermodynamic data (air temperature, pressure, and relative humidity). The iMet-XF system digitized signals from multiple sensors that were then passed through the Coyote's autopilot and transmitted to the P-3 for recording. Sea surface temperature was also measured near the end of each flight using an infrared sensor.

At times, instrument challenges occurred during these flights. For example, thermodynamic data were unusable for roughly half of the missions conducted. Because the aircraft were not recovered following each flight, the root causes of these issues are unknown. Work is currently being done to integrate new and improved instrument packages into the next generation of air-launched sUAS for hurricane research, including a multi-hole turbulence probe, improved thermodynamic and infrared sensors, and a laser or radar altimeter system to provide information on ocean waves and to more accurately measure the height of the aircraft above the sea.

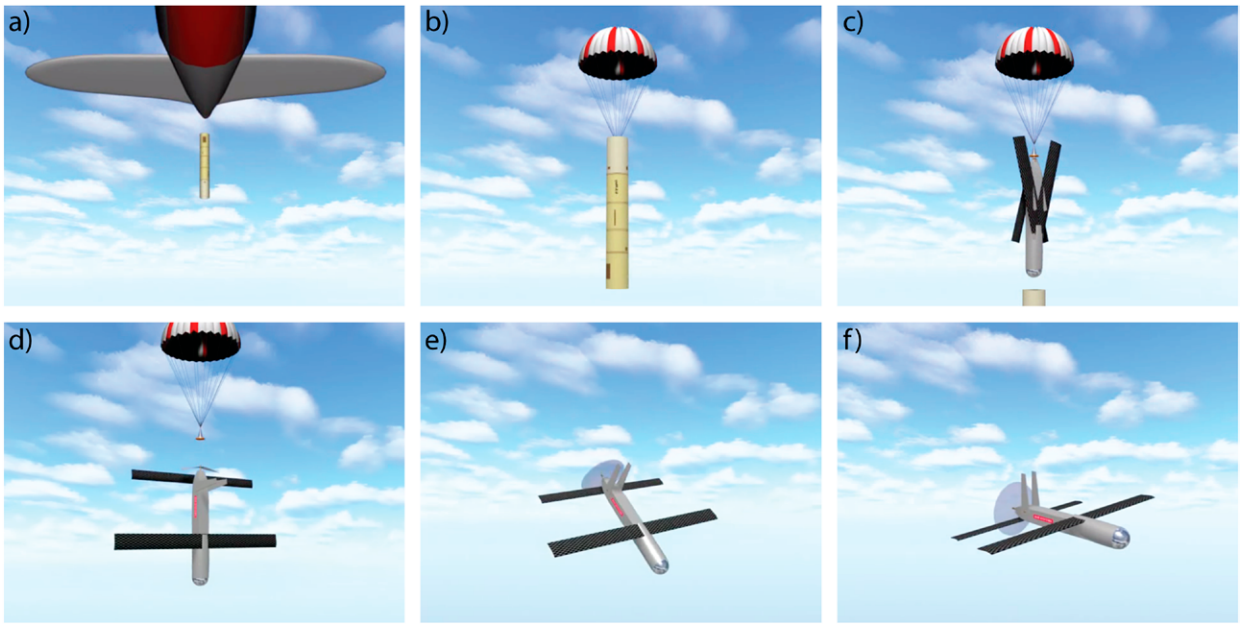

Fig. 2. A depiction of the Coyote sUAS launch sequence. (a) A Coyote is released in a sonobuoy canister from a NOAA P-3 aircraft. (b) A parachute initially slows the descent. (c) The canister falls away and the Coyote wings and stabilizers deploy. (d) After the Coyote is in an operational configuration, the parachute releases. (e) The motor starts and the Coyote levels out. (f) The Coyote attains level flight and begins operations. Images were captured from a video provided courtesy of Raytheon Corporation.

canister is released, and the Coyote wings and stabilizers unfold (Fig. 2c). When the Coyote is in its operational configuration with wings and stabilizers fully deployed, it detaches from the parachute (Fig. 2d) and the motor starts (Fig. 2e). The Coyote then levels out and begins operations (Fig. 2f). The version of the Coyote for this work had a battery supporting ~1 h of endurance, although flights in highly turbulent environments and loss of communications often lead to shorter missions. Similar to dropsondes, the Coyote is considered expendable and is not recovered after descending into the ocean at the end of a flight.

The Coyote has an advanced autopilot system that controls the aircraft in flight (see sidebar), with an operator on board the NOAA P-3 sending instructions via a two-way radio connection. Using a workstation on the P-3 (Fig. 1c), this operator monitors real-time meteorological information and can send waypoint and altitude commands to the Coyote to conduct targeted sampling (Fig. 1d).

In 2017–18, seven successful Coyote flights were executed in major Atlantic hurricanes. Six of these flights were conducted in Hurricane Maria when it was east of the Bahamas and was slowly weakening from a category 3 to a category 2 hurricane (Fig. 3a). The seventh flight was in Hurricane Michael (2018) when it was intensifying from a category 3 to a category 4 hurricane (Fig. 3b).

Flight patterns. Like other experiments utilizing NOAA's P-3 aircraft, these missions were conducted using procedures described in the NOAA Hurricane Research Division annual Hurricane Field Program.[1] Several "modules" for the Small Unmanned Aerial Vehicle Experiment (SUAVE) were conceived and documented in advance. The two specific modules that were conducted during the Hurricane Maria and Michael flights were the "eyewall" and the "inflow" modules.

For the eyewall module, the Coyote is launched in a hurricane's eye and is then directed toward the eyewall for an eventual circumnavigation (Fig. 4a), ideally at the radius of maximum winds (RMW). During the circumnavigation, the Coyote typically descends incrementally, making continuous measurements at various altitudes at the RMW. Although ascent is also possible with the Coyote, it is usually avoided due to the increased battery usage. The primary goal of the eyewall module is to more accurately measure the extent of the maximum winds azimuthally and vertically.

[1] More information on NOAA's Hurricane Field Program is available at www.aoml.noaa.gov/hrd/programs_sub/HFP.html.

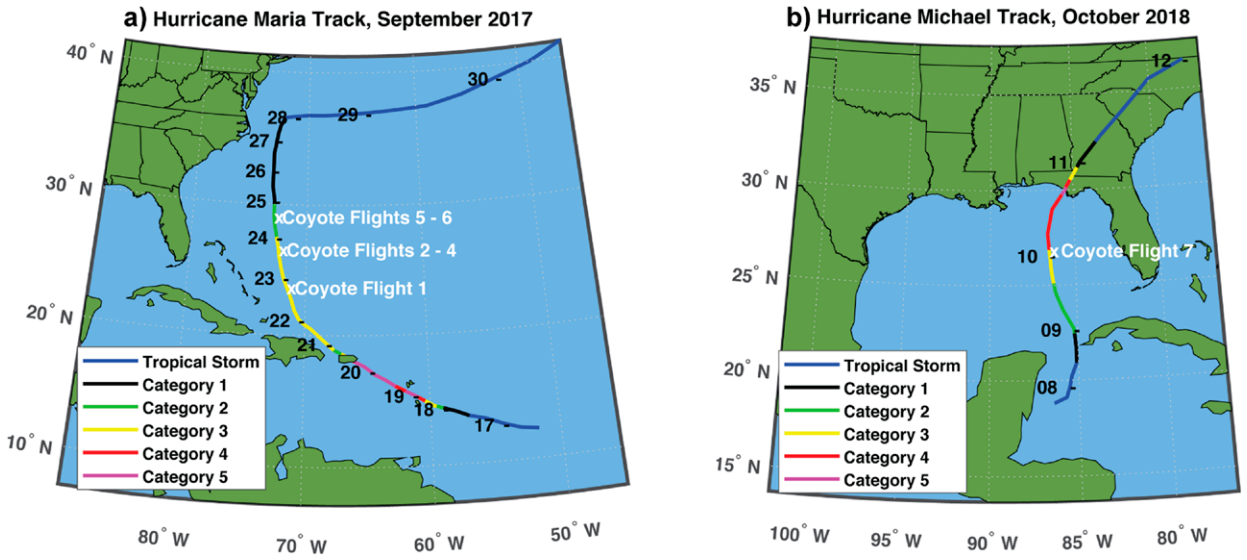

Fig. 3. National Hurricane Center best track of Hurricanes (a) Maria (2017) and (b) Michael (2018), colored based on the storm intensity. The 0000 UTC storm location of each date is indicated by black text along with the approximate locations of the Coyote missions in white text.

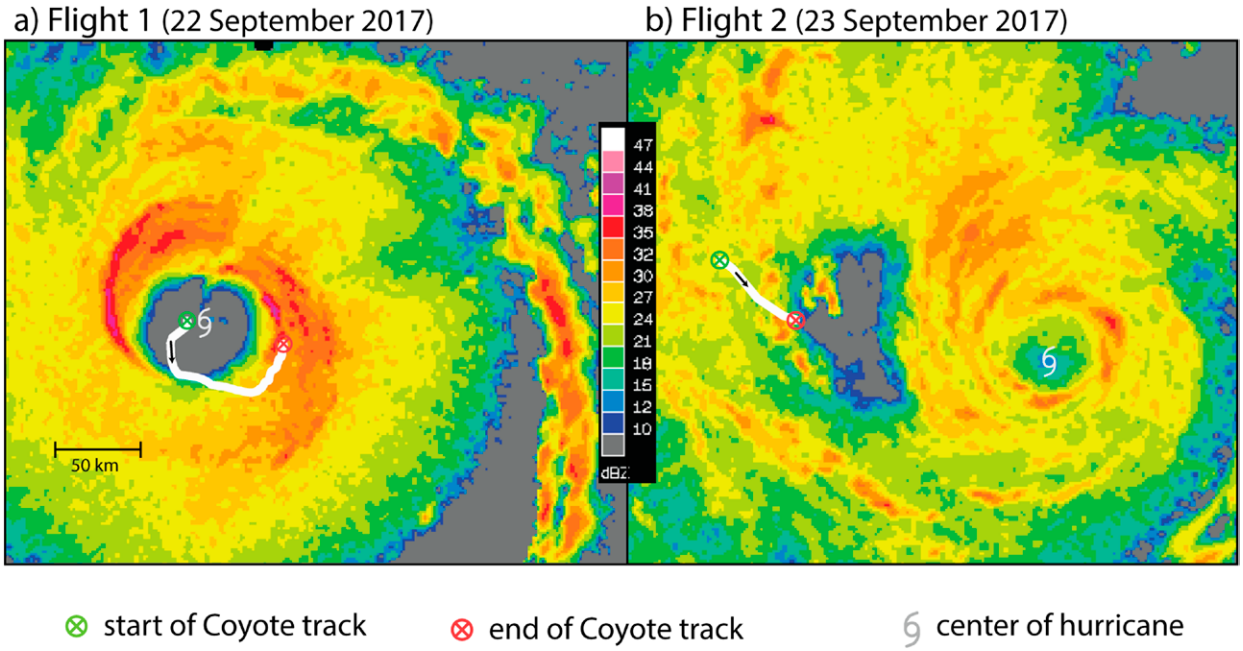

Fig. 4. Sample tracks from two Coyote flights (white lines) in Hurricane Maria (2017) overlaid on reflectivity from the NOAA P-3 lower fuselage radar. (a) Flight 1, showing an example of an eyewall mission with radar data valid 2111 UTC 22 Sep, and (b) flight 2, showing an example of an inflow mission with radar data valid 1851 UTC 23 Sep.

The inflow module is a two-part operation that involves launching the Coyote well outside of the storm's inner core, in a region expected to coincide with the azimuth of maximum near-surface inflow. The Coyote then flies radially inward (Fig. 4b), eventually reaching the hurricane eyewall where it can fly a pattern similar to that of the eyewall module. The primary purpose of the inflow module is to measure vertical fluxes of momentum, heat, and moisture in the hurricane boundary layer and to determine kinematic properties of the TC boundary layer such as the magnitude of near-surface inflow velocity.

Communication between the Coyote and the P-3 is a critical part of these operations. The maximum range of communication between the Coyote and P-3 is roughly 25 km. This range dictates the flight plan for the NOAA P-3 while a Coyote is in the air. An example P-3 flight track during Coyote flight 3 is shown in Fig. 5b. During an eyewall module, the P-3 typically crosses into and out of the hurricane eye, and flies downwind just outside the eyewall, to maintain relatively small horizontal separation from the Coyote.

Mission planning. Due to the complexity of releasing an sUAS in the TC inner core, each deployment required different mission planning. The strategies relied on proper sUAS placement while maintaining communication between the P-3 and sUAS for the ~1 h duration of each module. To optimize each mission, software was developed to automate, and potentially modify, flight paths quickly. The ability to change the flight paths during a given mission was crucial, as some TC characteristics (e.g., radius of maximum winds, storm asymmetry) could only be determined by using other P-3 instrumentation in real time. This capability allowed for flexibility when conducting missions from the P-3 aircraft.

For Hurricane Maria (2017) operations, mission planning began on 20 September 2017, after the storm made landfall in Puerto Rico. The forecast for Maria included a slow reintensification, peaking on 22 September before maintaining near-steady intensity through 24 September. Maria's clear, 40-nautical-mile-wide eye (1 nautical mile = 1.852 km) would provide a safe region for maneuvering the P-3 while the sUAS was prepared and deployed from the aircraft. During the sequence of missions in Maria, both eyewall and inflow experiments were executed.

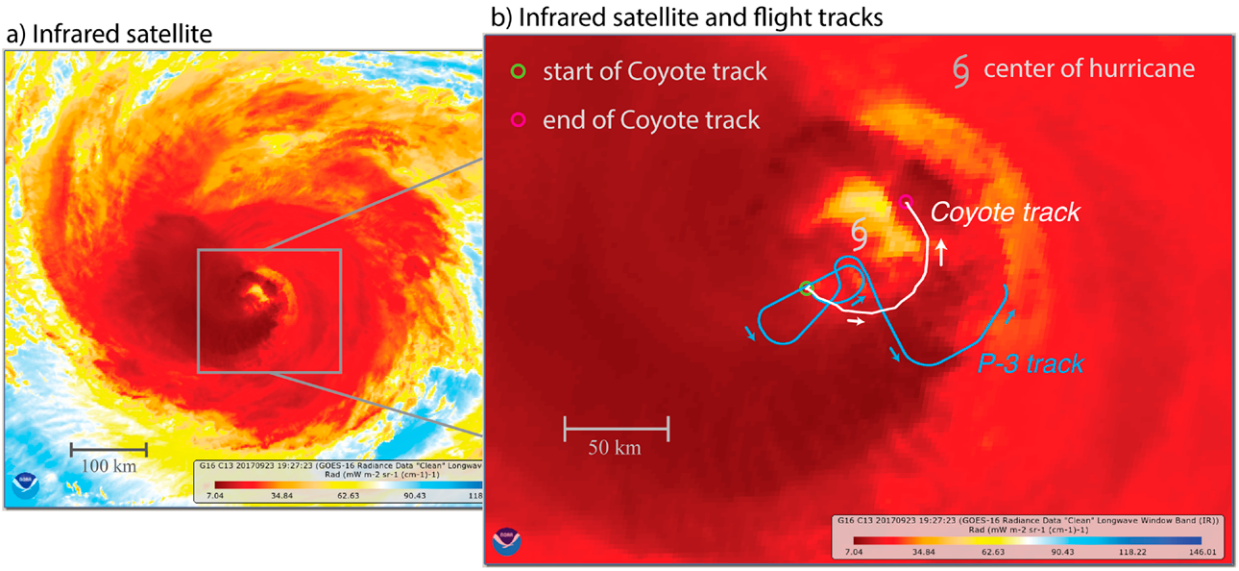

Fig. 5. Infrared satellite images of Hurricane Maria at 1927 UTC 23 Sep 2017. The image on the right shows the center of the hurricane and the tracks of Coyote flight 3 (white) and the NOAA P-3 (blue) from 1925 to 1957 UTC.

In Hurricane Michael (2018), only one Coyote aircraft was available. Its mission was to measure eyewall conditions near the location of maximum winds during a period of intensification. Planning for this mission began several days in advance, when the National Hurricane Center (NHC) indicated a high chance of tropical cyclogenesis in the western Caribbean. The initial Coyote flight pattern was created assuming an asymmetric vortex, with maximum winds located in the northeast quadrant of the storm. This plan was adjusted based on aircraft reconnaissance data collected during the missions prior to the sUAS launch. Data showed that the eye was too small for the P-3 to circumnavigate while the Coyote sampled the eyewall, which required the original flight plan to be modified such that Coyote operations began after the P-3 completed all of its operational reconnaissance requirements (e.g., storm center fixes and vortex-scale sampling).

Highlights of missions in Hurricanes Maria (2017) and Michael (2018). Table 1 provides an overview of the 2017–18 Coyote flights, while a summary of altitudes and wind speed measurements are shown in Fig. 6. Most missions featured level flight (i.e., nearly constant altitude), which are advantageous for computing turbulence properties. For two cases (flights 5 and 6), the Coyote motor failed to start. Nevertheless, both aircraft were able to maintain controlled flight during these so-called "glider missions," as useful measurements were collected en route from the eye to the eyewall as the sUAS made a slow descent to the ocean surface. Some highlights of Coyote operations within Hurricanes Maria and Michael are listed in Table 1. Altogether, 161.5 min of sUAS data were collected, primarily within the hurricane PBL at altitudes below 1 km MSL. It should also be noted that these data will be made publicly available via NOAA/AOML's Hurricane Research Division web page soon after publication.

Turbulence within hurricanes

This section summarizes some of the analyses being conducted with Coyote sUAS data. Although multiple scientific foci are being investigated, these preliminary analyses focus on turbulence using high-frequency in situ wind data.

High-frequency wind measurements. Throughout the hurricane deployments discussed above, the Coyote sUAS demonstrated an ability to maintain autopilot-controlled flight in

Table 1. Summary of Coyote sUAS flights in the 2017–18 seasons.

Flight No.	Date	Type of mission	Duration of data collection (min)	Maximum horizontal wind speed (m s^{-1})	Notes
1	22 Sep 2017	Eyewall	40.9	63.6	Longest flight (40.9 min) Peak downdraft (–13.8 m s^{-1} at 126 m MSL) Lowest maintained altitude (136 m MSL for 240 s)
2	23 Sep 2017	Inflow	30.0	38.8	Sampled boundary layer within hurricane rainbands
3	23 Sep 2017	Eyewall	31.6	69.5	Most data points from one flight (4,642)
4	23 Sep 2017	Eyewall	32.4	51.9	One of three flights (along with flights 1 and 3) to travel more than 90 km
5	24 Sep 2017	Eyewall glider	6.1	46.5	Engine failed to start Up to 10 Hz data
6	24 Sep 2017	Eyewall glider	7.0	47.6	Engine failed to start Up to 10 Hz data
7	10 Oct 2018	Eyewall	13.5	87.0	Peak horizontal wind speed (87.0 m s^{-1} at 641 m MSL) Peak updraft (+14.4 m s^{-1} at 624 m MSL)

winds up to 87 m s^{-1}. Moreover, the autopilot's software reported the aircraft's roll, pitch, and yaw along with GPS-based three-component position and ground speed. Airborne wind measurements are usually made with a multi-hole probe (MHP; e.g., van den Kroonenberg et al. 2008; Leise et al. 2013). The Coyote, however, had only a Pitot-static system (P/s). The Pitot-static algorithm (Rautenberg et al. 2018) designed for use with such instrumentation was found to by typically unsuitable for turbulence calculations due to excessive noise. Fortunately, spectral analysis illustrated that the autopilot kept the P/s aligned with incident airstream on scales longer than 3 s (90 m at airspeed 30 m s^{-1}),[2] a scale comparable to that for P-3 measurements in the eyewalls of Hurricanes Allen and Hugo (Zhang et al. 2011b). An expanded description and evaluation of the procedure for determining high-frequency wind calculations is in preparation.

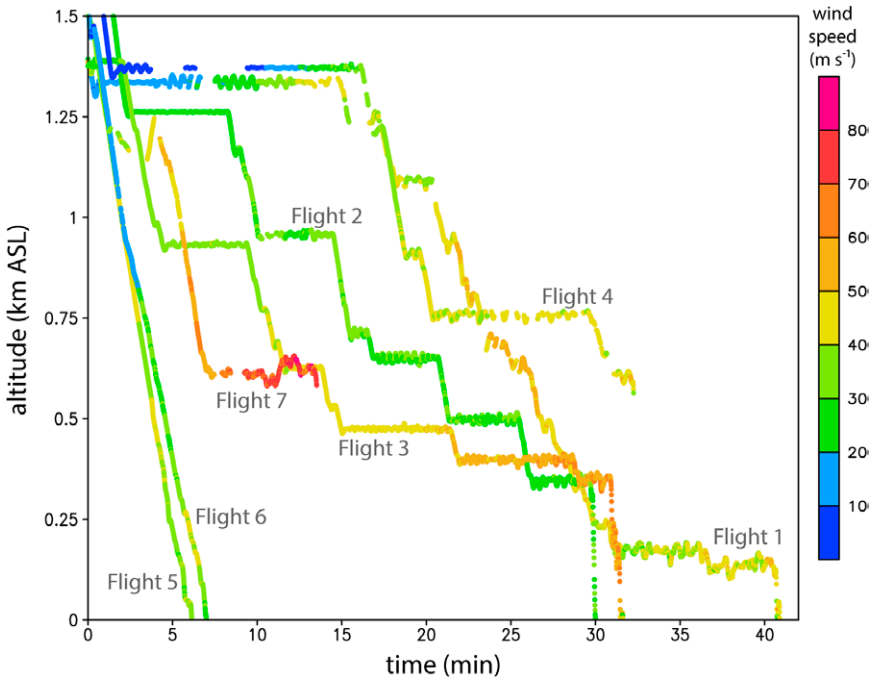

Fig. 6. Summary of all wind speed data collected during Coyote sUAS flights in 2017–18 (colored dots, m s^{-1}) as a function of time and height above sea level (ASL). Flights 1–4 and 7 were typical "stepped descent" flight patterns, while flights 5–6 were "glider" flights.

Wind speeds estimated by this technique provide initial estimates of turbulence properties in the hurricane boundary layer that can be compared to previous flights in the hurricane PBL from the P-3 aircraft. For example, in Hurricane Michael (Fig. 7), the altitude over the flight leg averaged 610 m MSL and varied between 580 and 650 m (Fig. 7b). Most notably, the values of tangential wind speed varied

[2] Scales smaller than 100 m (0.3 Hz) were evidently contaminated by aircraft motion. That is, the P/s was not aligned with the airstream, probably due to a "Dutch roll."

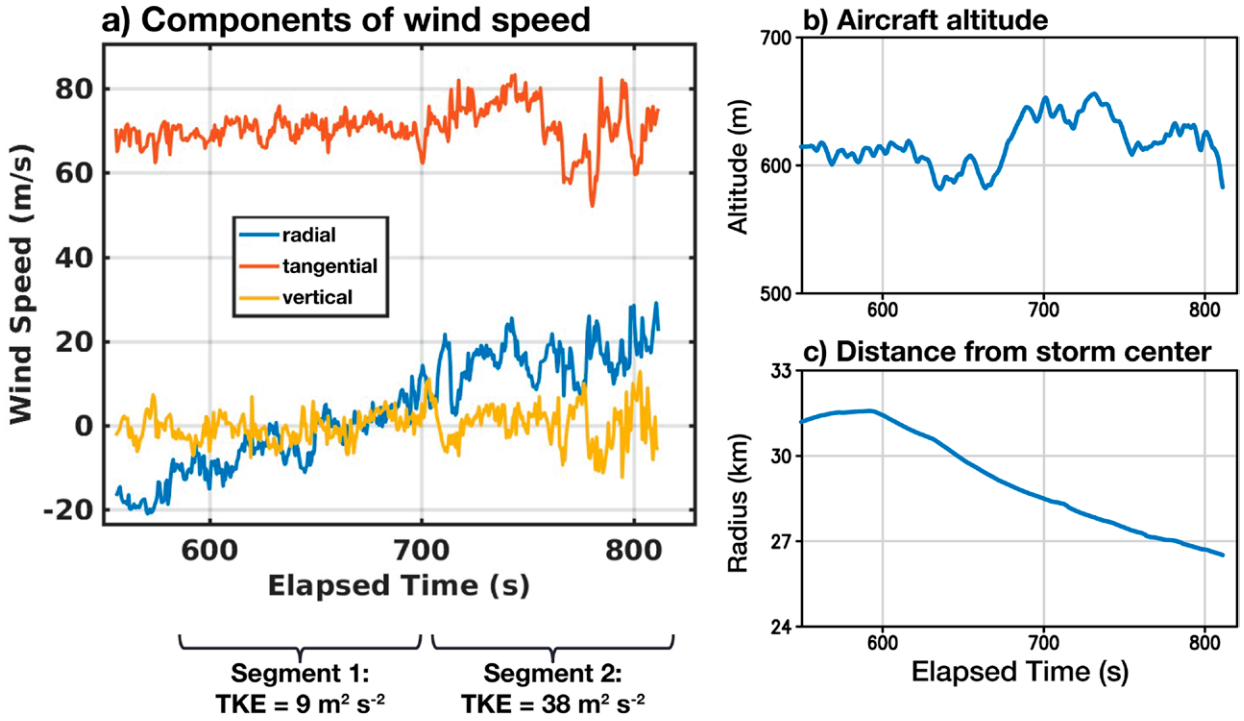

Fig. 7. Time series of flight-level data near the end of flight 7 in Hurricane Michael. (a) The three components of wind speed in cylindrical coordinates, as indicated in the legend. The turbulent nature of winds in the hurricane eyewall is apparent. Values of TKE during two segments are listed at the bottom of the panel. (b) Aircraft altitude, illustrating nearly level flight (i.e., near-constant altitude). (c) Distance from the center of the hurricane, showing how the Coyote sUAS gradually moved toward the center of the hurricane during this segment of the flight.

between 54 and 86 m s^{-1}, and averaged 72 m s^{-1} (Fig. 7a). Assuming a reduction factor of 75% for the adjustment of these winds from the 600-m level to the 10-m level [Table 2 of Franklin et al. (2003), assuming a 925-mb flight level], the estimated maximum sustained 10-m wind speed was 54 m s^{-1}, which corresponds well with the NHC best track value of 56.6 m s^{-1} (110 kt; 1 kt ≈ 0.5144 m s^{-1}) at this time (Beven et al. 2019).

Turbulence kinetic energy (TKE) is estimated from two segments of the flight 7 data, each 2 min long as illustrated at the bottom of Fig. 7. For the earlier segment, TKE is estimated to be 9 m^2 s^{-2}, which is comparable to the largest values determined from X-band Doppler radar data by Lorsolo et al. (2010). For the later segment, estimated TKE is much larger: 38 m^2 s^{-2}. It is noteworthy that this sUAS maintained nearly level flight in such conditions.

Other notable features of these data include updrafts *and* downdrafts exceeding 10 m s^{-1} (yellow data in Fig. 7a) within the hurricane boundary layer, which is consistent with previous measurements from other platforms (e.g., Marks et al. 2008; Stern et al. 2016). Another interesting feature of Fig. 7a is that the radial velocity changed from negative values (denoting inflow) to positive values (denoting outflow) at approximately 680 s into the flight. Also, during this time, the sUAS was gradually moving toward smaller radius (Fig. 7c), that is, it was moving closer to the hurricane eye. These are important points for interpretation of turbulence fluctuations, such as the abrupt increase in TKE at this time, as discussed below.

Comparison with previous studies. A limited number of previous studies have measured turbulence properties in the PBL of hurricanes. Most notable is the CBLAST experiment (Black et al. 2007), in which the NOAA P-3 was instrumented with special gust probes including NOAA's Best Aircraft Turbulence (BAT) probe sampling at 50 Hz (Dobosy et al. 2013). However, all of these flights were conducted far from the hurricane center in tropical-storm-force wind

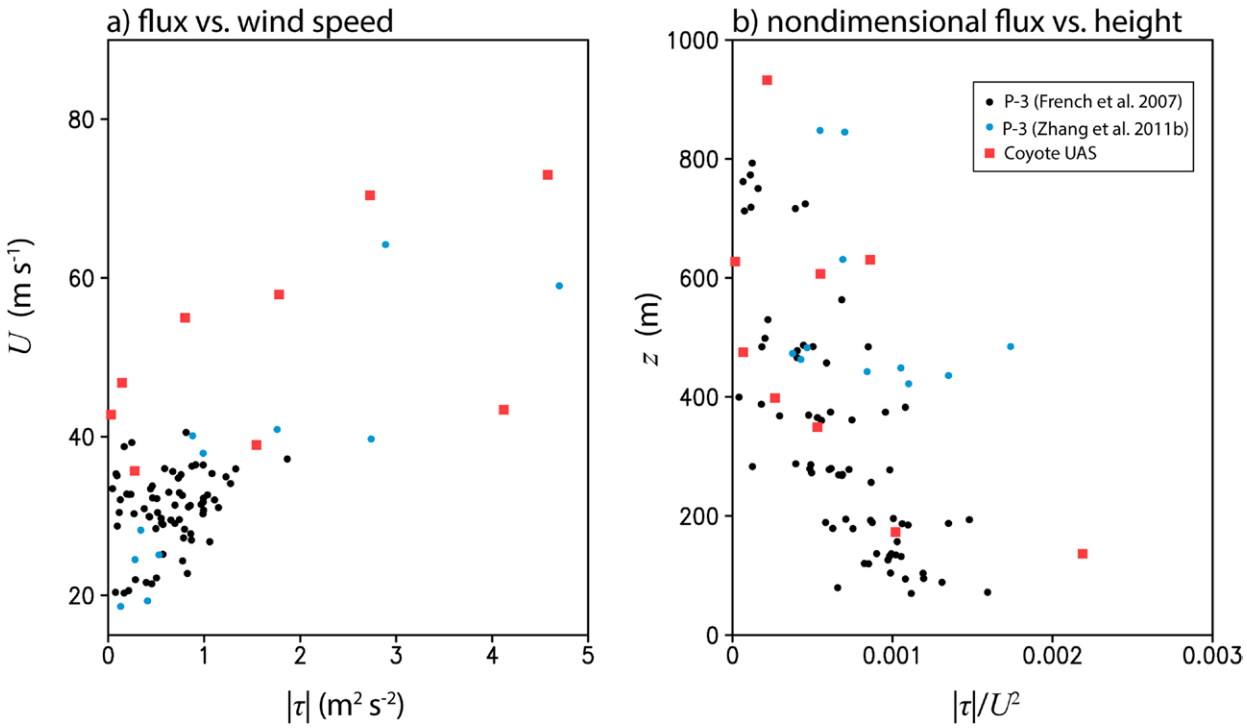

Fig. 8. Scatterplots of the magnitude of turbulence momentum flux, $|\tau| = [\langle u'w' \rangle^2 + \langle v'w' \rangle^2]^{1/2}$, from Coyote sUAS flights in 2017–18 (red) and from previous NOAA P-3 flights as determined by French et al. (2007) (black) and Zhang et al. (2011b) (blue). (a) Momentum flux vs mean wind speed U, showing how the Coyote sUAS flights operated at higher wind speeds compared to most P-3 flights. (b) Nondimensional momentum flux vs height, highlighting the similarity between the Coyote sUAS and P-3 measurements.

speeds (10-m wind speed <33 m s^{-1}). French et al. (2007) described these data and provided values of turbulence momentum flux magnitude, where brackets indicate an average value of a variable over some time period, and primes indicate perturbations from that average; for example, along a level flight leg, a variable $\alpha(t)$ can be expressed as $\alpha(t) = \langle \alpha \rangle + \alpha'(t)$.

More recently, Zhang et al. (2011b) examined data from unusually low-level flights into major Hurricanes Allen (1980) and Hugo (1989) using the NOAA P-3. These flights were as low as 422 m and measured winds in the inner core of these hurricanes, including within the high-wind eyewall. Estimates of $|\tau|$ were calculated using the same method as French et al. (2007), but for flight-level wind speeds as high as 64 m s^{-1}.

These previously published data can be compared with Coyote sUAS data. To that end, nearly level flight legs containing high-frequency data and few data dropouts were identified in the Coyote sUAS dataset. Nine flight segments from three flights (flights 1, 3, and 7) were identified for further calculation. As in previous studies (French et al. 2007; Zhang et al. 2011b), the flight-level winds were decomposed into a mean and fluctuations.

A scatterplot of the estimates of $|\tau|$ from the Coyote sUAS flights, as a function of average flight-level wind speed U (Fig. 8a), demonstrates that reasonable values are determined when compared with estimates from previous studies. A few of the sUAS measurements have similar values of U as the CBLAST measurements (i.e., $U \approx 40$ m s^{-1}) and, encouragingly, exhibit similar values of $|\tau|$. The same conclusion is drawn from a comparison of sUAS measurements with P-3 measurements at higher wind speeds ($U \approx 60$ m s^{-1}) from Zhang et al. (2011b).

The same data, normalized by U^2 and plotted as a function of height MSL (Fig. 8b), show similarly encouraging agreement between the P-3 flights and sUAS flights, showing an overall increase in $|\tau|$ downward from 400 m as expected for shear-dominated boundary layer turbulent flow (e.g., Lenschow 1970; Nicholls 1985; Stull 1988; Tjernström and Smedman 1993). Extrapolating these results downward to the surface yield nondimensional surface

stress values between 1.2 and 2.5 × 10^{-3}. Similar values were determined at hurricane-force wind speeds, using a different method, by Bell et al. (2012), although they reported values up to 50% larger.

In the future, we plan to also examine the distribution of radial turbulence fluxes, for example, $\langle u'v' \rangle$, which are especially important in the eyewall of hurricanes because they act to limit maximum hurricane intensity (Bryan and Rotunno 2009; Rotunno and Bryan 2012; Zhang et al. 2018). Only a few studies have presented observed radial turbulence fluxes in hurricane eyewalls (e.g., Zhang and Montgomery 2012; Guimond et al. 2018). An interesting result of these studies is that radial momentum fluxes can have the same magnitude as vertical momentum fluxes in the eyewall of hurricanes; our preliminary calculations with Coyote sUAS data show the same result (not shown). We also plan to estimate eddy diffusivities in the hurricane boundary layer using the sUAS data, as done with P-3 data by Zhang et al. (2011b), Zhang and Drennan (2012), and Zhang and Montgomery (2012).

Comparison and synergy with large-eddy simulations. Some other results from our analyses of flight-level Coyote data are notable. For example, the change from inflow to outflow during flight 7 (Fig. 7a) requires explanation. Additionally, the preliminary diagnosis of components (i.e., radial and tangential) of vertical turbulence momentum fluxes sometimes had the opposite sign compared to those in a simple shear-driven PBL.

To help place these high-frequency observations into better context of the overall hurricane structure, Coyote observations have been compared to output from a novel large-eddy simulation (LES) of an idealized hurricane (Worsnop et al. 2017b; Stern and Bryan 2018). This simulation uses Cloud Model 1 (CM1; Bryan and Fritsch 2002) with 31-m horizontal grid spacing and 15.6-m vertical grid spacing, which allows for resolved-scale turbulent flow (Fig. 9a) and therefore does not use a PBL parameterization. The simulated storm is smaller and more intense than the hurricanes sampled with the Coyote sUAS. Nevertheless, the LES produces realistic mesoscale structure in the eyewall region compared to observational analyses of mature hurricanes [cf. Figs. 9c,d with Zhang et al. (2011a)]. Hence, the spatial distribution of turbulence processes in the LES is expected to be similar to that in actual hurricanes, and this overall distribution (but not the magnitude) of turbulence properties is the focus for interpreting the high-frequency sUAS observations below.

The analyses in Figs. 9b–d utilize average fields (denoted by angled brackets) as determined by temporally averaging 1-min model output over the fourth hour of the simulation. Perturbations were defined as differences from the 3D time-averaged field, for example, $v'(x, y, z, t) = v(x, y, z, t) - \langle v \rangle \langle x, y, z \rangle$. Results were then azimuthally averaged and presented in cylindrical coordinates.

Of key interest in the simulated storm is the eyewall, which is simply defined by $\langle w \rangle = +1$ m s^{-1} (dashed purple contours in Fig. 9). The eyewall is clearly the most turbulent region of the storm (Fig. 9b), although there is a tendency for locally higher values of TKE in the inner half of the eyewall, a pattern consistent with observational studies (e.g., Lorsolo et al. 2010). Since the Coyote sUAS was gradually moving toward smaller radii near the end of flight 7 (Fig. 7c), it was likely measuring from the outer edge toward the inner edge of the eyewall, as indicated by the black arrows in Fig. 9. Notably, the average radial velocity changes from negative to positive in this region (Fig. 9c), consistent with sUAS observations (Fig. 7a), although it is possible that the sUAS encountered either a storm-motion induced asymmetry or a mesoscale vortex that is not present in the simulation. Nevertheless, the simulation captures processes in the hurricane eyewall that can explain aspects of the sUAS data. For instance, an airplane flying a constant altitude, as indicated by the arrow in Fig. 9d, should experience a change in the sign of the vertical flux of tangential velocity $\langle v'w' \rangle$ from weakly negative to strongly positive; this variation in flux is associated with the change in sign of

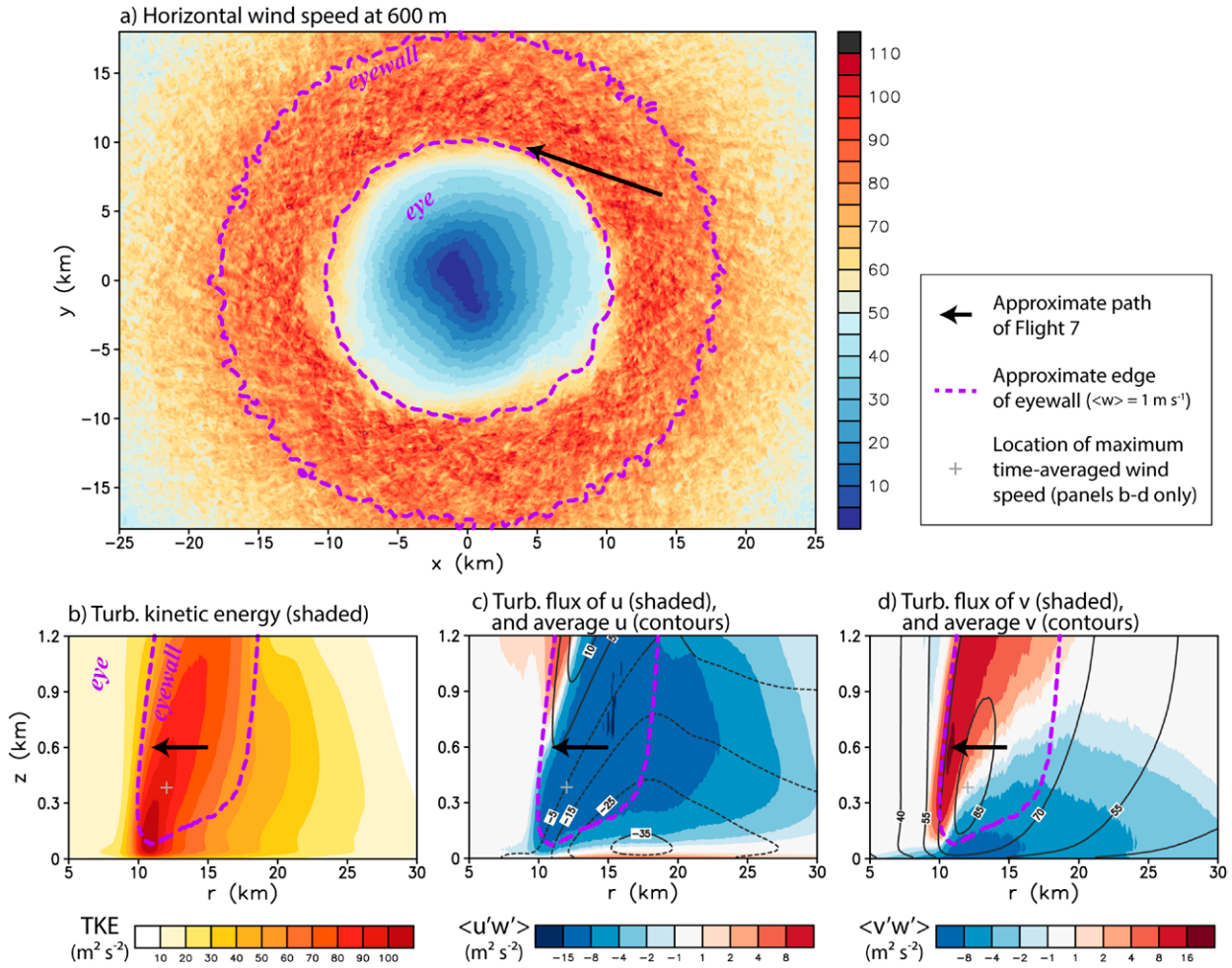

Fig. 9. Output from an LES of an idealized hurricane. In all panels, the arrow approximates the Coyote's path near the end of flight 7 in Hurricane Michael (final ≈ 200 s depicted in Fig. 7), and the dashed purple contour (showing average vertical velocity of +1 m s^{-1}) indicates the approximate location of the hurricane eyewall. (a) Instantaneous horizontal wind speed at z = 600 m, illustrating the turbulent nature of the hurricane eyewall. (b) TKE (shaded) showing that the most-turbulent flow is along the inner edge of the eyewall. (c) Analysis of the average radial velocity ($\langle u \rangle$, contours every 10 m s^{-1}) and its vertical turbulence flux ($\langle u'w' \rangle$, shaded); this component of momentum flux is typically negative, except very near the surface and at the inner edge of the eyewall. (d) Analysis of the average tangential velocity ($\langle v \rangle$, contours every 15 m s^{-1}) and its vertical turbulence flux ($\langle v'w' \rangle$, shaded); this component of momentum flux is generally negative outward of the maximum winds, but is positive inward of the maximum winds.

the vertical gradient of $\langle v \rangle$ from the outer portion of the eyewall (where $\delta\langle v \rangle/\delta z > 0$) to the inner portion of the eyewall (where $\delta\langle v \rangle/\delta z < 0$). The LES output also shows that the vertical flux of radial velocity $\langle u'w' \rangle$ would be expected to decrease in magnitude along the flight leg from strongly negative to near zero in this region (Fig. 9c). These inferences from LES are consistent with Coyote observations (not shown). Hence, LES output can be instrumental in placing observational data into context of the overall storm structure that may otherwise be difficult to understand. Although most of these results are consistent with simple eddy-diffusivity models based on "*K*-theory" (e.g., Tennekes and Lumley 1972), the LES output shows that some regions of the hurricane boundary layer have countergradient momentum fluxes (not shown). Countergradient momentum fluxes can also occur in coarser-resolution models of hurricanes (e.g., Persing et al. 2013) but, to the authors' knowledge, have not yet been documented using observations in hurricanes.

These analyses of a hurricane LES demonstrate the complexity of turbulence properties in the boundary layer of hurricane eyewalls. They also illustrate the extremely turbulent

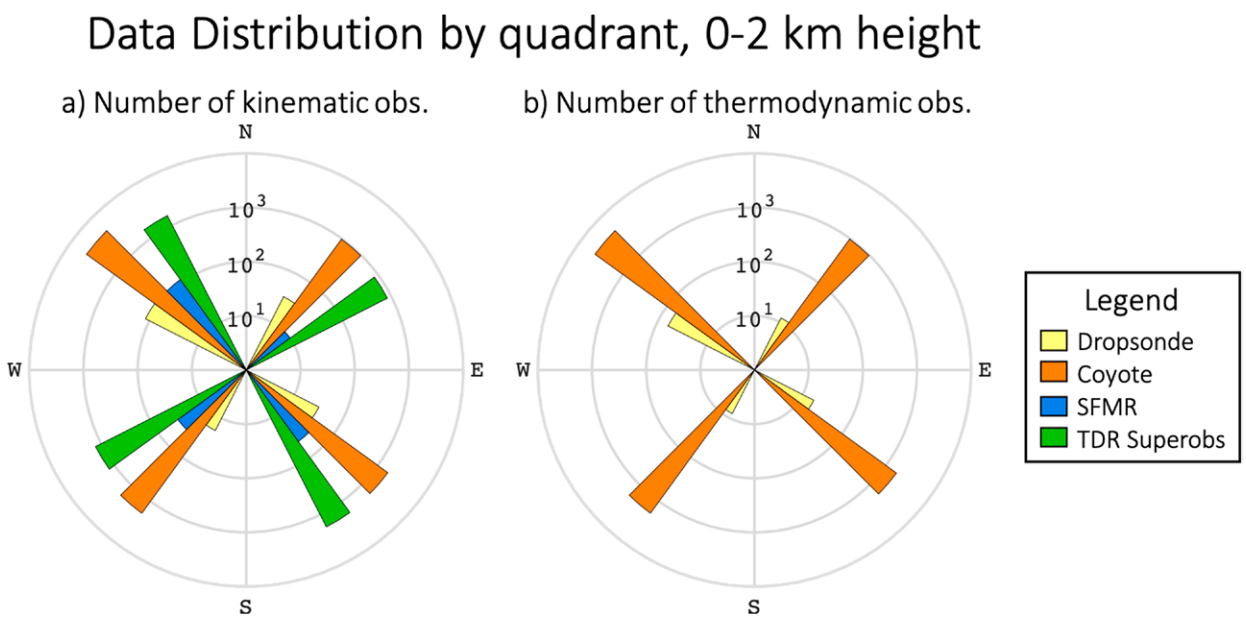

Fig. 10. Number of observational data points, plotted by quadrant and using a logarithmic scale, in the lowest 2 km from Hurricane Maria on 23 Sep 2017. (a) Number of kinematic observations (i.e., velocity measurements) and (b) number of thermodynamic observations (i.e., temperature and humidity measurements). "SFMR" refers to the Stepped Frequency Microwave Radiometer, and "TDR" refers to the P-3 Tail Doppler Radar. This analysis shows that the Coyote sUAS flights provide a similar amount of kinematic data near the surface as the P-3 Doppler radar, but provide a substantially greater amount of thermodynamic data than any other instrument.

nature of the hurricane eyewall, consistent with observational studies (e.g., Aberson et al. 2006b; Marks et al. 2008; Stern et al. 2016). Perhaps most important for future work, the LES output suggests operations for additional sUAS flights. For example, missions focused on boundary layer turbulence would benefit from flights located just radially outward of the eyewall where mesoscale flow patterns are simpler and TKE is smaller. Such flights would enable more straightforward analysis of turbulence properties and would represent a lower-risk flight area for small aircraft.

Data impact and the evaluation of operational forecast models

Numerical weather prediction (NWP) is a key element of hurricane forecasting, and advances in prediction systems result from advances in both the accuracy of the underlying models and the assimilation of observational data. The Coyote sUAS data provide a unique opportunity to conduct groundbreaking research in both of these areas.

To illustrate the unique value of sUAS data for improving NWP of TCs, Fig. 10 shows the number of data points below 2 km MSL collected by NOAA P-3 flights into Hurricane Maria on 23 September 2017. This layer includes the highest wind speeds in hurricanes and spans the entire PBL. In terms of kinematic observations (i.e., velocity measurements), the TDR on board the NOAA P-3 typically provides the greatest amount of data within hurricanes, and the Hurricane Maria flight was no exception (see green bars in Fig. 10a). However, the Coyote sUAS flights on this day provided a similar amount of data (orange bars in Fig. 10a). Even though the aerial coverage of the Coyote measurements is much more limited than the P-3 TDR, the Coyote measurements include data within the hurricane's eye where the TDR cannot measure winds because precipitation is typically low.

A unique aspect of sUAS flights is best highlighted in Fig. 10b, which shows that the Coyote sUAS flights provided, by far, the greatest amount of thermodynamic observations (i.e., measurements of pressure, temperature, and humidity). In every quadrant of Hurricane Maria, Coyote sUAS flights (orange bars in Fig. 10b) provided at least an order of magnitude

more thermodynamic observations than dropsondes (yellow bars), and, in some quadrants, there are two orders of magnitude more sUAS data than dropsonde data.

In summary, the large number of measurements of both kinematic and thermodynamic Coyote sUAS observations in the PBL of Hurricane Maria, along with how they are distributed spatially as shown in Figs. 4–6, suggest that positive impacts could be obtained when they are assimilated in numerical models that can resolve relevant atmospheric features.

Evaluation of HWRF boundary layer. The HWRF system (e.g., Biswas et al. 2017) is NOAA's primary operational modeling system for the prediction of TCs. Unique observations, particularly those from aircraft, have played a crucial role in previous improvements made to the HWRF model physics (e.g., Zhang et al. 2015). Safety concerns related to the operation of manned aircraft within the hurricane PBL make sUAS like the Coyote an attractive option for the collection of data needed to evaluate the HWRF PBL scheme and to develop further improvements.

Coyote sUAS flight 3 (Fig. 5b) completed a partial orbit of Maria's eyewall, providing an opportunity to evaluate thermodynamic conditions in a strong-wind environment and to compare the observations to model-derived fields from the simulated eyewall. To perform this comparison, retrospective forecasts of Hurricane Maria were made with the 2017 operational HWRF configuration. Eight different model cycles were selected for analysis, with forecast hours that ranged from 0 to 120 h. All of the forecasts had a valid time of 1800 UTC 23 September 2017, ~1 h prior to the sUAS flight. To avoid penalizing the model for errors in hurricane track and size, both the sUAS observations and the model output were regridded by normalizing the radial coordinate by RMW. The sUAS trajectory (in normalized coordinates) was then recreated in the simulations so that the azimuths and heights sampled in the model simulations were the same as the ones sampled in the observed storm. Both the actual and simulated sUAS trajectories followed the RMW, minimizing structural differences between the regions of the observed and simulated storms.

Scatterplots of observed versus simulated air and dewpoint temperatures for the analysis cycle and for the 72-h forecast cycle are shown in Fig. 11. This comparison reveals a clear correlation between the observed and simulated air and dewpoint temperatures. However, the HWRF conditions are consistently 1°–2°C cooler and drier than the sUAS observations (~300–1,400 m MSL). The cooler conditions are most pronounced within the mid-PBL regions, suggesting that the model exhibits a lower static stability relative to the observed lapse rate. Other forecast cycles exhibited similar behavior (not shown). To determine whether the sUAS observations were in error, temperature and dewpoint profiles from dropsondes deployed from the same flight were also examined and were found to be similar to the sUAS data (not shown).

These model biases have important implications for the representation of air–sea fluxes, lower boundary layer stability, and the accuracy of hurricane intensity change predictions. Although accurate track, intensity, and wind radii forecast guidance from HWRF is the primary goal for the modeling system, improvements in the representation of physical processes are also a priority. Further HWRF model evaluation and development efforts using these sUAS data are ongoing. An important question is whether the thermodynamic biases in the eyewall that are documented here also extend radially outward within the hurricane. If they are present throughout the storm, the radial gradients of temperature and moisture may be approximately correct, potentially reducing the impact of these biases on storm intensity. Investigation of the observed and simulated radial gradients will need to account for differences in the location of outer convective bands in the observed and simulated storms, which can substantially modulate the local thermodynamic structure of the storm (e.g., Kepert et al. 2016).

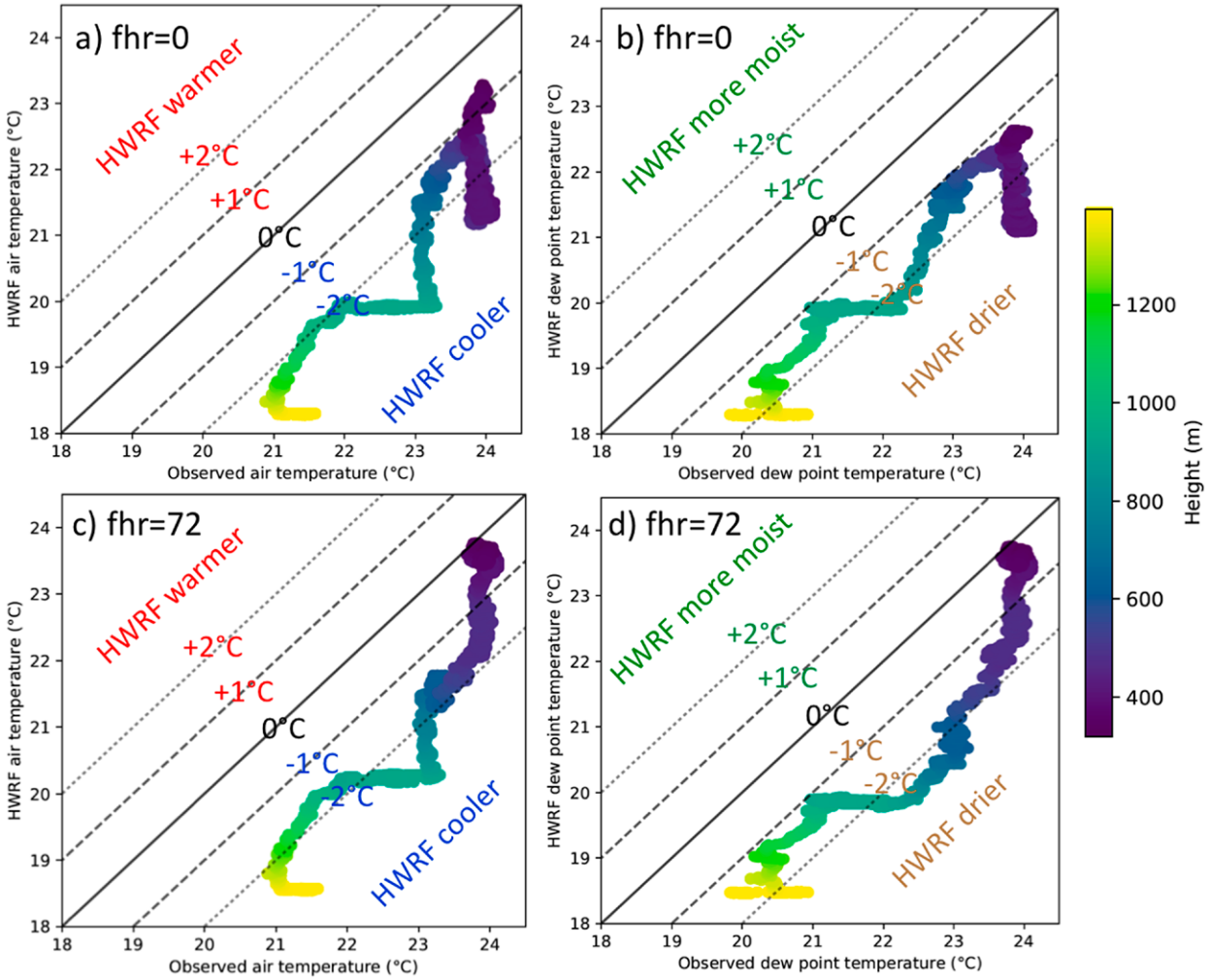

Fig. 11. Scatterplots comparing the Coyote-observed (*x* coordinate) and HWRF-simulated (*y* coordinate) (a),(c) air temperature and (b),(d) dewpoint temperature. Colors indicate the height of the data. (top) The HWRF initialization from the 1800 UTC 23 Sep 2017 model cycle, and (bottom) the 72-h forecast from the 1800 UTC 20 Sep 2017 model cycle. The Coyote data show that HWRF had a cool, dry, and potentially unstable bias in the boundary layer.

Data impact. Data assimilation is the process of utilizing a statistical technique to combine observations with a numerical model forecast with the goal of obtaining the best estimate of the state of the atmosphere. As computing power has increased exponentially in the last four decades (e.g., Moore 2006), capabilities of numerical models and data assimilation systems for weather prediction purposes have also improved dramatically. However, observations are very limited in the inner core of a hurricane, where strong winds and extreme turbulence make data collection difficult.

To evaluate the ability of sUAS data to impact the analyzed structure of Hurricane Maria, the Hurricane Ensemble Data Assimilation System (HEDAS; Aksoy et al. 2012, 2013) is utilized. This system was developed by NOAA specifically to assimilate hurricane inner-core observations at the vortex scale using HWRF. Here, the Coyote sUAS case of 1800 UTC 23 September 2017 was chosen. One experiment assimilated horizontal wind, temperature, and specific humidity observations from Coyote flights 2–4, plus 1) radial wind superobservations (superobs) from the TDR, 2) kinematic and thermodynamic observations at P3 flight level and by dropwindsonde, 3) 10-m wind speed retrieved from the Stepped Frequency Microwave Radiometer (SFMR; Uhlhorn et al. 2007), and 4) horizontal winds from the atmospheric motion vectors system (AMV; Velden et al. 2005). To isolate the effects of the Coyote data, a second experiment assimilated measurements 1–4, but not those from the sUAS.

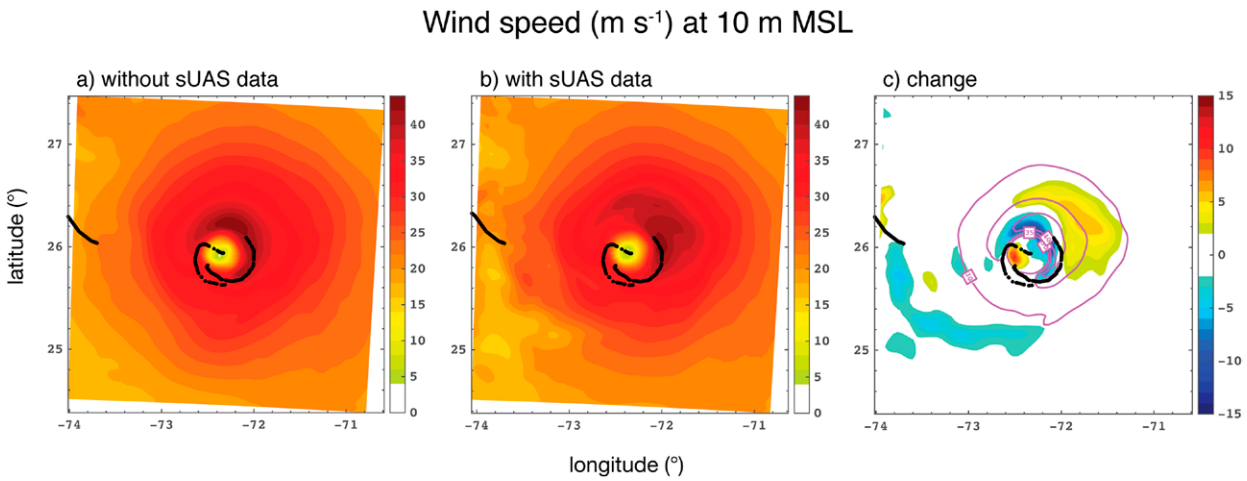

Fig. 12. Preliminary results from data analysis experiments of Hurricane Maria on 23 Sep 2017. (a) An analysis of 10-m wind speed without Coyote sUAS data, (b) an analysis with Coyote sUAS data, and (c) the change in 10-m wind speed (shaded) and 10-m wind speed from the analysis without sUAS data (purple contours). In all panels, the black dots denote locations of sUAS data. The primary change after assimilating sUAS data are an outward shift of the eyewall in the northeast quadrant of the hurricane, and a decrease in wind speed in the southwest quadrant.

Preliminary results for an analysis of wind speed at 10 m MSL are shown in Fig. 12. Using all data except those from the Coyote (Fig. 12a), an asymmetric wind structure is apparent, with the maximum winds in the north-northeast part of the eyewall. Including sUAS data results in a shift in the location of the maximum winds to the eastern part of the eyewall (Fig. 12b). The northeastern sections of the eyewall clearly demonstrate the effects of the sUAS data, with a shift in the maximum winds tens of kilometers away from the Coyote flight track, and an expansion of the region of strongest winds. For the inflow flight (flight 2) to the west of the storm center, the sUAS data act to decrease the winds for nearly 200 km downstream of the flight location (Fig. 12c). Plans for future work include forecasts from this time forward to see how the modified storm structure affects the HWRF forecasts of Hurricane Maria. The limited number of cases available with Coyote observations render it infeasible to carry out such an analysis at this time.

Summary

The Coyote is a small, air-launched unmanned aircraft that was deployed from the NOAA P-3 in Hurricanes Maria (2017) and Michael (2018). The aircraft collected kinematic and thermodynamic data in the boundary layer of both hurricanes. For the seven sUAS missions, wind observations were sent in near–real time to NHC forecasters. The >1 Hz measurements below 150 m within the eyewall of Hurricane Maria are the first in situ measurements of this kind because of inherent dangers with flying a manned aircraft at such low altitudes and high wind speeds (up to 87 m s^{-1}).

The measurements from Hurricanes Maria and Michael have been used to estimate turbulence characteristics within the hurricane eyewall. Values of the magnitude of turbulence momentum flux are encouragingly similar to previous measurements using the NOAA P-3 manned aircraft and provide confidence in the ability of an sUAS to collect reliable data in hurricane conditions. These data also allow for an evaluation of how well numerical models simulated the boundary layers of Hurricanes Maria and Michael, and can potentially lead to improvements in the PBL and surface-layer parameterizations of numerical models. Additionally, Coyote data assimilation experiments demonstrated the ability of sUAS measurements to alter the distribution of winds in a simulated storm, thereby potentially reducing uncertainties associated with the initialization of forecasts for storm position, intensity and structure.

In the future, sUAS might allow for targeting regions of hurricanes where numerical models have large uncertainty and where direct measurements are rare. Further work is also being done to develop the next generation of sUAS. Efforts are currently underway to expand current capabilities by enhancing payload capacity, augmenting battery life, and increasing the transmission range so that the NOAA P-3 is not required to loiter nearby. Even without these future advancements in hand, the existing sUAS concept of operations provides the ability to obtain unique datasets that are likely to enhance the community's understanding of hurricane boundary layer structure and intensity change.

Acknowledgments. This work was originally funded by an award to the National Oceanic and Atmospheric Administration (NOAA) from the Disaster Relief Appropriations Act of 2013 (also known as the "Sandy Supplemental"). Additional resources were provided by NOAA's Office of Marine and Aviation Operations and by the Assistant Administrator of NOAA's Office of Oceanic and Atmospheric Research. The authors appreciate the hard work by staff at NOAA's Aircraft Operations Center; these sUAS flights could not have been possible without their assistance. George Bryan was supported by the National Center for Atmospheric Research (NCAR), which is a major facility sponsored by the National Science Foundation (NSF) under Cooperative Agreement 1852977. High-performance computing support from Cheyenne (doi:10.5065/D6RX99HX) was provided by NCAR's Computational and Information Systems Laboratory. Additional high-performance computing resources were provided by the NOAA Research and Development High Performance Computing Program (http://rdhpcs.noaa.gov). Work completed by Gijs de Boer was supported by the NOAA Physical Sciences Division, the NOAA Unmanned Aircraft Systems Program Office, the NSF (OPP 1836423), and U.S. Department of Energy (DE-SC0013306). Joshua Wadler was supported by the NSF Graduate Research Fellowship under Grant DGE-1451511. Evan Kalina was supported by funding from NOAA Award NA17OAR4320101. Jun Zhang was supported by NOAA Grant NA14NWS4680028, and NSF Grants AGS1822128 and ASG1654831. Partial funding support was provided through the Cooperative Agreement NA67RJ0149 between NOAA and the University of Miami. The Developmental Testbed Center (DTC) is funded by NOAA, the U.S. Air Force, NCAR, and the NSF. Xiaomin Chen was supported by a National Research Council (NRC) Research Associateship award.

References

Aberson, S. D., M. L. Black, R. A. Black, R. W. Burpee, J. J. Cione, C. W. Landsea, and F. D. Marks, 2006a: Thirty years of tropical cyclone research with the NOAA P-3 aircraft. *Bull. Amer. Meteor. Soc.*, **87**, 1039–1056, https://doi.org/10.1175/BAMS-87-8-1039.

——, M. T. Montgomery, M. Bell, and M. Black, 2006b: Hurricane Isabel (2003): New insights into the physics of intense storms. Part II: Extreme localized wind. *Bull. Amer. Meteor. Soc.*, **87**, 1349–1354, https://doi.org/10.1175/BAMS-87-10-1349.

Aksoy, A., S. Lorsolo, T. Vukicevic, K. J. Sellwood, S. D. Aberson, and F. Zhang, 2012: The HWRF Hurricane Ensemble Data Assimilation System (HEDAS) for high-resolution data: The impact of airborne Doppler radar observations in an OSSE. *Mon. Wea. Rev.*, **140**, 1843–1862, https://doi.org/10.1175/MWR-D-11-00212.1.

——, S. D. Aberson, T. Vukicevic, K. J. Sellwood, S. Lorsolo, and X. Zhang, 2013: Assimilation of high-resolution tropical cyclone observations with an ensemble Kalman filter using NOAA/AOML/HRD's HEDAS: Evaluation of the 2008–11 vortex-scale analyses. *Mon. Wea. Rev.*, **141**, 1842–1865, https://doi.org/10.1175/MWR-D-12-00194.1.

Bell, M. M., M. T. Montgomery, and K. A. Emanuel, 2012: Air–sea enthalpy and momentum exchange at major hurricane wind speeds observed during CBLAST. *J. Atmos. Sci.*, **69**, 3197–3222, https://doi.org/10.1175/JAS-D-11-0276.1.

Beven, J. L., II, R. Berg, and A. Hagen, 2019: Hurricane Michael (AL142018). National Hurricane Center Tropical Cyclone Rep., 86 pp., www.nhc.noaa.gov/data/tcr/AL142018_Michael.pdf.

Biswas, M. K., and Coauthors, 2017: Hurricane Weather Research and Forecasting (HWRF) model: 2017 Scientific Documentation. NCAR Tech. Note NCAR/TN-544+STR, 99 pp., https://doi.org/10.5065/D6MK6BPR.

Black, P. G., and Coauthors, 2007: Air–sea exchange in hurricanes: Synthesis of observations from the Coupled Boundary Layer Air–Sea Transfer experiment. *Bull. Amer. Meteor. Soc.*, **88**, 357–374, https://doi.org/10.1175/BAMS-88-3-357.

Braun, S. A., and W.-K. Tao, 2000: Sensitivity of high-resolution simulations of Hurricane Bob (1991) to planetary boundary layer parameterizations. *Mon. Wea. Rev.*, **128**, 3941–3961, https://doi.org/10.1175/1520-0493(2000)129<3941:SOHRSO>2.0.CO;2.

Bryan, G. H., 2012: Effects of surface exchange coefficients and turbulence length scales on the intensity and structure of numerically simulated hurricanes. *Mon. Wea. Rev.*, **140**, 1125–1143, https://doi.org/10.1175/MWR-D-11-00231.1.

——, 2013: Comments on 'Sensitivity of tropical-cyclone models to the surface drag coefficient.' *Quart. J. Roy. Meteor. Soc.*, **139**, 1957–1960, https://doi.org/10.1002/qj.2066.

——, and J. M. Fritsch, 2002: A benchmark simulation for moist nonhydrostatic numerical models. *Mon. Wea. Rev.*, **130**, 2917–2928, https://doi.org/10.1175/1520-0493(2002)130<2917:ABSFMN>2.0.CO;2.

——, and R. Rotunno, 2009: The maximum intensity of tropical cyclones in axisymmetric numerical model simulations. *Mon. Wea. Rev.*, **137**, 1770–1789, https://doi.org/10.1175/2008MWR2709.1.

Cascella, G., J. J. Cione, E. W. Uhlhorn, and S. J. Majumdar, 2008: Inner-core characteristics of Ophelia (2005) and Noel (2007) as revealed by Aerosonde data. *28th Conf. on Hurricanes and Tropical Meteorology*, Orlando, FL, Amer. Meteor. Soc., 7C.4, https://ams.confex.com/ams/28Hurricanes/techprogram/paper_137864.htm.

Chen, X., Y. Wang, J. Fang, and M. Xue, 2018: A numerical study on rapid intensification of Typhoon Vicente (2012) in the South China Sea. Part II: Roles of inner-core processes. *J. Atmos. Sci.*, **75**, 235–255, https://doi.org/10.1175/JAS-D-17-0129.1.

Cione, J. J., and Coauthors, 2008: The first successful unmanned aerial system (UAS) mission into a tropical cyclone (Ophelia 2005). *12th Conf. on Integrated Observing and Assimilation Systems for Atmosphere, Ocean, and Land Surface (IOAS-AOLS)*, New Orleans, LA, Amer. Meteor. Soc., 15B.4, https://ams.confex.com/ams/88Annual/techprogram/paper_135142.htm.

——, E. A. Kalina, J. A. Zhang, and E. W. Uhlhorn, 2013: Observations of air–sea interaction and intensity change in hurricanes. *Mon. Wea. Rev.*, **141**, 2368–2382, https://doi.org/10.1175/MWR-D-12-00070.1.

——, ——, E. W. Uhlhorn, A. M. Farber, and B. Damiano, 2016: Coyote unmanned aircraft system observations in Hurricane Edouard (2014). *Earth Space Sci.*, **3**, 370–380, https://doi.org/10.1002/2016EA000187.

Dobosy, R., and Coauthors, 2013: Calibration and quality assurance of an airborne turbulence probe in an aeronautical wind tunnel. *J. Atmos. Oceanic Technol.*, **30**, 182–196, https://doi.org/10.1175/JTECH-D-11-00206.1.

Drennan, W. M., J. A. Zhang, J. R. French, C. McCormick, and P. G. Black, 2007: Turbulent fluxes in the hurricane boundary layer. Part II: Latent heat flux. *J. Atmos. Sci.*, **64**, 1103–1115, https://doi.org/10.1175/JAS3889.1.

Elston, J., B. Argrow, M. Stachura, D. Weibel, D. Lawrence, and D. Pope, 2015: Overview of small fixed-wing unmanned aircraft for meteorological sampling. *J. Atmos. Oceanic Technol.*, **32**, 97–115, https://doi.org/10.1175/JTECH-D-13-00236.1.

Emanuel, K. A., 1995: Sensitivity of tropical cyclones to surface exchange coefficients and a revised steady-state model incorporating eye dynamics. *J. Atmos. Sci.*, **52**, 3969–3976, https://doi.org/10.1175/1520-0469(1995)052<3969:SOTCTS>2.0.CO;2.

——, 2005: *Divine Wind: The History and Science of Hurricanes*. Oxford University Press, 296 pp.

Franklin, J. L., M. L. Black, and K. Valde, 2003: GPS dropwindsonde wind profiles in hurricanes and their operational implications. *Wea. Forecasting*, **18**, 32–44, https://doi.org/10.1175/1520-0434(2003)018<0032:GDWPIH>2.0.CO;2.

French, J., W. Drennan, J. Zhang, and P. Black, 2007: Turbulent fluxes in the hurricane boundary layer. Part I: Momentum flux. *J. Atmos. Sci.*, **64**, 1089–1102, https://doi.org/10.1175/JAS3887.1.

Gall, R., J. Franklin, F. Marks, E. N. Rappaport, and F. Toepfer, 2013: The Hurricane Forecast Improvement Project. *Bull. Amer. Meteor. Soc.*, **94**, 329–343, https://doi.org/10.1175/BAMS-D-12-00071.1.

Guimond, S. R., J. A. Zhang, J. W. Sapp, and S. J. Frasier, 2018: Coherent turbulence in the boundary layer of Hurricane Rita (2005) during an eyewall replacement cycle. *J. Atmos. Sci.*, **75**, 3071–3093, https://doi.org/10.1175/JAS-D-17-0347.1.

Harper, B. A., J. D. Kepert, and J. D. Ginger, 2010: Guidelines for converting between various wind averaging periods in tropical cyclone conditions. WMO/TD-1555, 54 pp., www.wmo.int/pages/prog/www/tcp/documents/WMO_TD_1555_en.pdf.

Hock, T. F., and J. L. Franklin, 1999: The NCAR GPS dropwindsonde. *Bull. Amer. Meteor. Soc.*, **80**, 407–420, https://doi.org/10.1175/1520-0477(1999)080<0407:TNGD>2.0.CO;2.

Holland, G. J., T. McGeer, and H. Youngren, 1992: Autonomous aerosondes for economical atmospheric soundings anywhere on the globe. *Bull. Amer. Meteor. Soc.*, **73**, 1987–1998, https://doi.org/10.1175/1520-0477(1992)073<1987:AAFEAS>2.0.CO;2.

Jorgensen, D. P., P. H. Hildebrand, and C. L. Frush, 1983: Feasibility test of an airborne pulse-Doppler meteorological radar. *J. Climate Appl. Meteor.*, **22**, 744–757, https://doi.org/10.1175/1520-0450(1983)022<0744:FTOAAP>2.0.CO;2.

Kepert, J. D., 2012: Choosing a boundary layer parameterization for tropical cyclone modeling. *Mon. Wea. Rev.*, **140**, 1427–1445, https://doi.org/10.1175/MWR-D-11-00217.1.

——, J. Schwendike, and H. Ramsay, 2016: Why is the tropical cyclone boundary layer not "well mixed"? *J. Atmos. Sci.*, **73**, 957–973, https://doi.org/10.1175/JAS-D-15-0216.1.

Klotzbach, P. J., S. G. Bowen, R. Pielke, and M. Bell, 2018: Continental U.S. hurricane landfall frequency and associated damage: Observations and future risks. *Bull. Amer. Meteor. Soc.*, **99**, 1359–1376, https://doi.org/10.1175/BAMS-D-17-0184.1.

Leise, J. A., J. Masters, and R. Dobosy, 2013: Wind measurement from aircraft. NOAA Tech. Memo. OAR ARL-266, 209 pp., http://doi.org/10.7289/V5/TM-OAR-ARL-266.

Lenschow, D. H., 1970: Aircraft measurements of planetary boundary layer structure. *J. Appl. Meteor.*, **9**, 874–884, https://doi.org/10.1175/1520-0450(1970)009<0874:AMOPBL>2.0.CO;2.

Lin, P., and C.-S. Lee, 2008: The eyewall-penetration reconnaissance observation of Typhoon Longwang (2005) with unmanned aerial vehicle, Aerosonde. *J. Atmos. Oceanic Technol.*, **25**, 15–25, https://doi.org/10.1175/2007JTECHA914.1.

Lorsolo, S., J. A. Zhang, F. Marks, and J. Gamache, 2010: Estimation and mapping of hurricane turbulent energy using airborne Doppler measurements. *Mon. Wea. Rev.*, **138**, 3656–3670, https://doi.org/10.1175/2010MWR3183.1.

Marks, F. D., P. G. Black, M. T. Montgomery, and R. W. Burpee, 2008: Structure of the eye and eyewall of Hurricane Hugo (1989). *Mon. Wea. Rev.*, **136**, 1237–1259, https://doi.org/10.1175/2007MWR2073.1.

Montgomery, M. T., and R. K. Smith, 2017: Recent developments in the fluid dynamics of tropical cyclones. *Annu. Rev. Fluid Mech.*, **49**, 541–574, https://doi.org/10.1146/annurev-fluid-010816-060022.

——, ——, and N. Van Sang, 2010: Sensitivity of tropical cyclone models to the surface drag coefficient. *Quar. Roy. Meteor.*, **136**, 1945–1953, https://doi.org/10.1002/qj.702.

Moore, G., 2006: Moore's law at 40. *Understanding Moore's Law: Four Decades of Innovation*, D. Brock, Ed., Chemical Heritage Foundation, 67–84.

Nicholls, S., 1985: Aircraft observations of the Ekman layer during the Joint Air-Sea Interaction Experiment. *Quart. J. Roy. Meteor. Soc.*, **111**, 391–426, https://doi.org/10.1002/qj.49711146807.

Nolan, D. S., J. A. Zhang, and D. P. Stern, 2009a: Evaluation of planetary boundary layer parameterizations in tropical cyclones by comparison of in-situ data and high-resolution simulations of Hurricane Isabel (2003). Part I: Initialization, maximum winds, and outer core boundary layer structure. *Mon. Wea. Rev.*, **137**, 3651–3674, https://doi.org/10.1175/2009MWR2785.1.

——, D. P. Stern, and J. A. Zhang, 2009b: Evaluation of planetary boundary layer parameterizations in tropical cyclones by comparison of in situ observations and high-resolution simulations of Hurricane Isabel (2003). Part II: Inner-core boundary layer and eyewall structure. *Mon. Wea. Rev.*, **137**, 3675–3698, https://doi.org/10.1175/2009MWR2786.1.

Persing, J., M. T. Montgomery, J. C. McWilliams, and R. K. Smith, 2013: Asymmetric and axisymmetric dynamics of tropical cyclones. *Atmos. Chem. Phys.*, **13**, 12 299–12 341, https://doi.org/10.5194/acp-13-12299-2013.

Pielke, R. A., Jr., and C. W. Landsea, 1998: Normalized hurricane damages in the United States: 1925–95. *Wea. Forecasting*, **13**, 621–631, https://doi.org/10.1175/1520-0434(1998)013<0621:NHDITU>2.0.CO;2.

——, and ——, 1999: La Niña, El Niño, and Atlantic hurricane damages in the United States. *Bull. Amer. Meteor. Soc.*, **80**, 2027–2033, https://doi.org/10.1175/1520-0477(1999)080<2027:LNAENO>2.0.CO;2.

——, J. Gratz, C. W. Landsea, D. Collins, M. A. Saunders, and R. Musulin, 2008: Normalized hurricane damages in the United States. *Nat. Hazards Rev.*, **9**, 29–42, https://doi.org/10.1061/(ASCE)1527-6988(2008)9:1(29).

Rautenberg, A., M. S. Graf, N. Wildmann, A. Platis, and J. Bange, 2018: Reviewing wind measurement approaches for fixed-wing unmanned aircraft. *Atmosphere*, **9**, 422, https://doi.org/10.3390/atmos9110422.

Rotunno, R., and G. H. Bryan, 2012: Effects of parameterized diffusion on simulated hurricanes. *J. Atmos. Sci.*, **69**, 2284–2299, https://doi.org/10.1175/JAS-D-11-0204.1.

Smith, R. K., and G. L. Thomsen, 2010: Dependence of tropical cyclone intensification on the boundary layer representation in a numerical model. *Quart. J. Roy. Meteor. Soc.*, **136**, 1671–1685, https://doi.org/10.1002/qj.687.

Stern, D. P., and G. H. Bryan, 2018: Using simulated dropsondes to understand extreme updrafts and wind speeds in tropical cyclones. *Mon. Wea. Rev.*, **146**, 3901–3925, https://doi.org/10.1175/MWR-D-18-0041.1.

——, ——, and S. D. Aberson, 2016: Extreme low-level updrafts and wind speeds measured by dropsondes in tropical cyclones. *Mon. Wea. Rev.*, **144**, 2177–2204, https://doi.org/10.1175/MWR-D-15-0313.1.

Stull, R. B., 1988: *An Introduction to Boundary Layer Meteorology*. Atmospheric and Oceanographic Sciences Library, Vol. 13, Kluwer Academic, 670 pp.

Tallapragada, V., C. Kieu, Y. Kwon, S. Trahan, Q. Liu, Z. Zhang, and I. Kwon, 2014: Evaluation of storm structure from the operational HWRF model during 2012 implementation. *Mon. Wea. Rev.*, **142**, 4308–4325, https://doi.org/10.1175/MWR-D-13-00010.1.

Tennekes, H., and J. L. Lumley, 1972: *A First Course in Turbulence*, MIT Press, 266 pp.

Tjernström, M., and A.-S. Smedman, 1993: The vertical turbulence structure of the coastal marine atmospheric boundary layer. *J. Geophys. Res.*, **98**, 4809–4826, https://doi.org/10.1029/92JC02610.

Uhlhorn, E. W., P. G. Black, J. L. Franklin, M. Goodberlet, J. Carswell, and A. S. Goldstein, 2007: Hurricane surface wind measurements from an operational stepped frequency microwave radiometer. *Mon. Wea. Rev.*, **135**, 3070–3085, https://doi.org/10.1175/MWR3454.1.

van den Kroonenberg, A., T. Martin, M. Buschmann, J. Bange, and P. Vörsmann, 2008: Measuring the wind vector using the autonomous mini aerial vehicle M2AV. *J. Atmos. Oceanic Technol.*, **25**, 1969–1982, https://doi.org/10.1175/2008JTECHA1114.1.

Velden, C. S., and Coauthors, 2005: Recent innovations in deriving tropospheric winds from meteorological satellites. *Bull. Amer. Meteor. Soc.*, **86**, 205–223, https://doi.org/10.1175/BAMS-86-2-205.

Wadler, J. B., J. A. Zhang, B. Jaimes, and L. K. Shay, 2018: Downdrafts and the evolution of boundary layer thermodynamics in Hurricane Earl (2010) before and during rapid intensification. *Mon. Wea. Rev.*, **146**, 3545–3565, https://doi.org/10.1175/MWR-D-18-0090.1.

Worsnop, R. P., G. H. Bryan, J. K. Lundquist, and J. A. Zhang, 2017a: Using large-eddy simulations to define spectral and coherence characteristics of the hurricane boundary layer for wind-energy applications. *Bound.-Layer Meteor.*, **165**, 55–86, https://doi.org/10.1007/s10546-017-0266-x.

——, J. K. Lundquist, G. H. Bryan, R. Damiani, and W. Musial, 2017b: Gusts and shear within hurricane eyewalls can exceed offshore wind turbine design standards. *Geophys. Res. Lett.*, **44**, 6413–6420, https://doi.org/10.1002/2017GL073537.

Wurman, J., and K. Kosiba, 2018: The role of small-scale vortices in enhancing surface winds and damage in Hurricane Harvey (2017). *Mon. Wea. Rev.*, **146**, 713–722, https://doi.org/10.1175/MWR-D-17-0327.1.

Zhang, J. A., and W. M. Drennan, 2012: An observational study of vertical eddy diffusivity in the hurricane boundary layer. *J. Atmos. Sci.*, **69**, 3223–3236, https://doi.org/10.1175/JAS-D-11-0348.1.

——, and M. T. Montgomery, 2012: Observational estimates of the horizontal eddy diffusivity and mixing length in the low-level region of intense hurricanes. *J. Atmos. Sci.*, **69**, 1306–1316, https://doi.org/10.1175/JAS-D-11-0180.1.

——, R. Rogers, D. Nolan, and F. Marks, 2011a: On the characteristic height scales of the hurricane boundary layer. *Mon. Wea. Rev.*, **139**, 2523–2535, https://doi.org/10.1175/MWR-D-10-05017.1.

——, F. D. Marks, M. Montgomery, and S. Lorsolo, 2011b: An estimation of turbulent characteristics in the low-level region of intense Hurricanes Allen (1980) and Hugo (1989). *Mon. Wea. Rev.*, **139**, 1447–1462, https://doi.org/10.1175/2010MWR3435.1.

——, D. S. Nolan, R. Rogers, and V. Tallapragada, 2015: Evaluating the impact of improvements in the boundary layer parameterization on hurricane intensity and structure forecasts in HWRF. *Mon. Wea. Rev.*, **143**, 3136–3155, https://doi.org/10.1175/MWR-D-14-00339.1.

——, J. J. Cione, E. Kalina, E. Uhlhorn, T. Hock, and J. Smith, 2017: Observations of infrared sea surface temperature and air-sea interaction in Hurricane Edouard (2014) using GPS dropsondes. *J. Atmos. Oceanic Technol.*, **34**, 1333–1349, https://doi.org/10.1175/JTECH-D-16-0211.1.

——, F. D. Marks, J. Sippel, R. Rogers, X. Zhang, S. Gopalakrishnan, Z. Zhang, and V. Tallapragada, 2018: Evaluating the impact of improvement in the horizontal diffusion parameterization on hurricane prediction in the operational Hurricane Weather Research and Forecasting (HWRF) Model. *Wea. Forecasting*, **33**, 317–329, https://doi.org/10.1175/WAF-D-17-0097.1.